

AD-A190 096

HIGH-TEMPERATURE INTERGRANULAR CRACK GROWTH IN
MARTENSITIC 2-1/4 CR-1MO STEEL (U) ATOMIC ENERGY
RESEARCH ESTABLISHMENT HARWELL (ENGLAND)

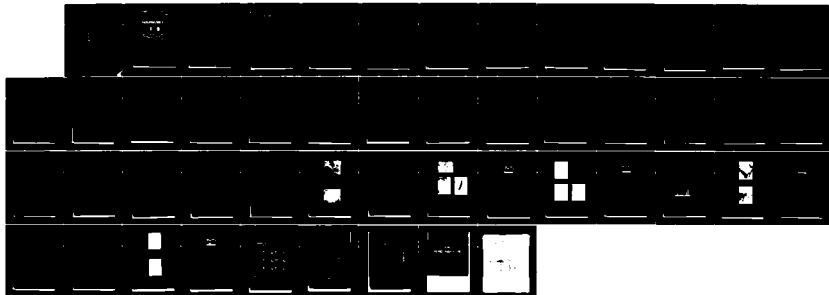
1/1

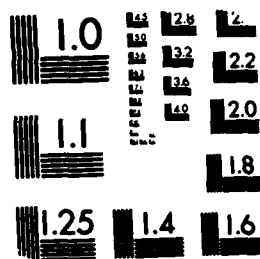
UNCLASSIFIED

C A HIPPSLEY ET AL. JAN 87 AERE-R-12464

F/G 11/6

NL





MICROCOPY RESOLUTION TEST CHART
NATIONAL BUREAU OF STANDARDS 1963-A

AERE R 12464

APPROVED FOR PUBLICATION

AERE R 12464

THIS DOCUMENT IS INTENDED FOR PUBLICATION IN THE OPEN LITERATURE.
Until it is published, it may not be circulated, or referred to outside the organization to
which copies have been sent.

DTIC FILE COPY

United Kingdom Atomic Energy Authority

HARWELL

DTIC
ELECTE
S JAN 11 1988 D
AD

**High-temperature intergranular
crack growth in martensitic
2 1/4 Cr-1 Mo steel**

DISTRIBUTION STATEMENT A
Approved for public release;
Distribution Unlimited

C A Hipsley* and P Bowen*

COPYRIGHT AND REPRODUCTION
Enquiries about copyright and reproduction should be addressed to the
Publications Office, AERE Harwell, Oxfordshire, England OX11 0RA.

*Dept of Metallurgy & Materials Science, University of Cambridge

*Materials Physics & Metallurgy Division

Harwell Laboratory, Oxfordshire OX11 0RA

January 1987

APPROVED FOR PUBLICATION

C14

HIGH-TEMPERATURE INTERGRANULAR CRACK
GROWTH IN MARTENSITIC 2½ Cr-1Mo STEEL

C A Hippsley* and P Bosen*

*Dept of Metallurgy & Materials Science, University of Cambridge.

*Materials Physics & Metallurgy Division
Harwell Laboratory

January 1987

HL86/1492 (C14)



Accession For	
NTIS GRA&I	<input checked="" type="checkbox"/>
DTIC TAB	<input type="checkbox"/>
Unannounced	<input type="checkbox"/>
Justification	
by	
Distribution	
Availability Codes	
Dist	Avail and/or Special
A-1	

87 12 28 079

HIGH-TEMPERATURE INTERGRANULAR CRACK
GROWTH IN MARTENSITIC 2½ Cr-1Mo STEEL

C A Hipsley and P Bowen

ABSTRACT

↙ Micromechanisms of high-temperature crack growth in martensitic 2½Cr-1Mo steel have been studied in vacuum, under static loading at 500°C. Detailed metallographic and fractographic measurements have been combined with Scanning Auger Microscopy and crack growth resistance curves to characterise the micro-mechanisms of failure.

At low stress intensities, less than $48-55 \text{ MPam}^{1/2}$, the mode of crack growth is high-temperature, brittle intergranular fracture (HTBIGF) and is controlled by the dynamic segregation of sulphur to crack-tip regions. Crack advance appears to occur by discrete jumps when a critical concentration of sulphur is achieved over the jump-distance. *Keywords: Brittle Fracture* ↘

At high stress intensities, greater than $48-55 \text{ MPam}^{1/2}$, the mode of fracture changes to intergranular microvoid coalescence (IGMVC), and is controlled by the distribution of sulphides. Of crucial importance are the relatively fine sulphides that reprecipitate from solid solution during the austenitising treatment.

The transition from HTBIGF to IGMVC is observed to occur over a critical range of stress intensity, and is accompanied by a steeper dependence of crack growth rate on stress-intensity. Both mechanisms of crack growth are encouraged by an increase in final austenitising temperature for a constant grain-size and scale of microstructure, through changes in the nature of sulphur in solution and small reprecipitated sulphides.

January 1987

CONTENTS

	<u>Page No.</u>
1. Introduction	5
2. Experimental	6
2.1 Material and heat treatment	6
2.2 Mechanical Testing	6
2.3 Metallography	7
2.4 Fractography	7
3. Results	8
3.1 Crack growth under monotonic loading	8
3.2 Metallography	10
3.3 Fractography	10
3.4 Auger electron spectroscopy	13
4. Discussion	14
4.1 High Temperature Brittle Intergranular Fracture (HTBIGF)	14
4.2 Intergranular Microvoid Coalescence (IGMVC)	17
4.3 The Transition from HTBIGF to IGMVC	18
4.4 Theoretical Model for HTBIGF	19
Conclusions	20
Acknowledgments	21
References	22

TABLES

Table

1 Composition of 2½Cr-1Mo plate, wt. %	24
2 Calculated size of plastic zone, r, and specimen size restrictions, $2.5(K/\sigma_o)^2$, as a function of applied stress intensity, K, at 500°C	24
3 Tensile properties measured for extremes of quenched conditions	25
4 Room temperature Vicker's hardness, $V_H(30 \text{ kg})$, as a function of tempering time at 500°C (standard deviations are in parentheses)	25
5 Quantitative analysis of fractographic features (standard deviations in parentheses)	26
6 Calculated size of crack opening displacement (δ) at 500°C, using $\delta = K^2(1 - \nu^2)/2\sigma_o E$, where $\nu = 0.3$, $\sigma_o = 840 \text{ MPa}$ and $E = 160 \text{ GPa}$ (26)	27
7 Equilibrium concentration (C_o) of sulphur in iron containing 0.53 Mn (wt. %)	27

CONTENTS (cont'd)

ILLUSTRATIONS

Fig.

- 1 Notched bend testpiece
- 2 Heat-treatment schedules
- 3 Crack growth resistance curves: stress intensity versus log (crack growth rate)
- 4 Crack growth resistance curves: log (stress intensity) versus log (crack growth rate)
- 5 Low magnification TEM micrograph of 1300-900 WQ condition
- 6 High magnification TEM micrograph of 1300 WQ condition
- 7 Measured size distribution of lath widths for 1300 WQ and 1300-900 WQ conditions
- 8 1300 WQ condition, $K = 40 \text{ MPam}^{1/2}$ (a) general area, (b) striations on individual grain boundary (direction of crack growth is arrowed) and (c) detail of individual striation arrowed
- 9 1300 WQ condition, $K = 60 \text{ MPam}^{1/2}$ (a) individual grain boundary showing microductility, (b) fine cavitation (around carbides, region A) and (c) coarse cavitation (around fine sulphides, region B)
- 10 EDS spectrum obtained from manganese sulphide inclusion ($\approx 200 \text{ nm}$)
- 11 Crack growth rate of $3.10^{-4} \text{ mm s}^{-1}$ (a) 1300 WQ condition and (b) 1300-900 WQ condition
- 12 Summary of observed dependence of fractographic features on (a) stress intensity and (b) crack growth rate
- 13 Auger electron spectra [$d^2(E)/d(E)$ versus E] obtained from (a) bulk intergranular facet and (b) intergranular facet located at the crack-tip
- 14 Comparison of fractographic features observed on grain boundaries (a) subjected to HTBIGF at 500°C (direction of crack growth arrowed) and (b) impact fracture at -196°C
- 15 Schematic representation of mechanisms of intergranular crack growth
- 16 Calculated coverage (F) versus applied stress intensity (K) for the range of quenched conditions
- 17 Calculated average concentration of sulphur (atomic %) required to promote grain boundary fracture for a range of applied stress intensity

1. Introduction

A number of recent papers have considered high temperature intergranular crack growth in low alloy steels in high-strength conditions (1-5). This type of cracking was originally seen following stress-relieving heat treatments applied after welding and was therefore named stress-relief-cracking or reheat-cracking (6-10). It is most commonly found in the coarse grained heat-affected-zones (HAZ's) which surround the weld-metal. Effects of HAZ microstructure have been studied in small scale testpieces by simulating the thermal-cycle experienced in a weldment. Comparative tests indicate that closely similar behaviour is found in full-scale weldments (11). Early efforts were directed at studying this phenomenon in stress-relaxation tests designed to parallel closely the conditions experienced by a weldment during post-weld-heat-treatments (PWHT). The results obtained were extremely useful in indicating the susceptibility of a particular alloy to stress-relief-cracking, but did not address the underlying mechanisms of crack growth in detail. Two distinct forms of intergranular cracking were identified, however, namely high temperature brittle intergranular fracture (HTBIGF) and intergranular microvoid coalescence (IGMVC). The former type of cracking has been associated with low temperatures (typically 300-500°C) and correspondingly high stresses when observed in stress relaxation tests, while the latter type of cracking has been associated with higher temperatures (typically 600-700°C) and correspondingly lower stresses when observed in stress relaxation tests.

More recently, attention has been directed towards characterising the underlying mechanisms of crack growth. It appears that the linear elastic stress intensity, K , can be used to characterise crack growth under static loading (2, 12). This is analogous to the use of the fatigue alternating stress intensity, ΔK , to characterise crack growth under cyclic loading.

The purpose of the present study is to address micromechanisms of high temperature intergranular crack growth. Experiments have been performed on well characterised martensitic microstructures, under constant load, ie increasing stress intensity, conditions. Particular attention has been given to the quantitative measurement of microstructural and fractographic features, and these observations are combined with mechanical test data and surface analysis, to establish micro-mechanisms of crack growth, and to assess a recent theoretical model for the solute enrichment of crack-tips(1).

2. Experimental

2.1 Material and heat treatment

All tests were performed on a commercial grade of 2% Cr-1Mo steel plate whose composition is given in Table 1. Notched-bend testpieces of the geometry shown in fig 1 were machined in the transverse - short-transverse (TST) orientation and heat-treated individually in a vacuum furnace with temperature control to $\pm 5^\circ\text{C}$. The heat-treatment schedules are shown in fig 2, and all initially involved austenitising at 1300°C for 30 minutes. This was followed by either direct water quenching, or furnace cooling to lower austenitising temperatures of 1200, 1100, 1000 and 900°C respectively, a 1 hour hold, and then a water quench.

2.2 Mechanical Testing

Static crack growth tests were carried out using a servo-hydraulic testing machine, equipped with a vacuum chamber and quartz lamp heating facilities. The test temperature was monitored by a thermocouple attached to the testpiece, and was maintained at $500 \pm 2^\circ\text{C}$. The test temperature was attained and stabilised within 15 minutes.

Tests were performed at nominal vacua of less than 10^{-4} mbar total pressure. Crack growth was measured by the DC potential drop technique. To avoid problems which are inherent to this technique when used for measuring crack growth rates under fatigue loading in vacuum (13) tests were performed at constant load (ie increasing stress intensity, K) conditions. Under static loading K has been used successfully to characterise the rate of crack growth with time, da/dt (2, 12), under decreasing stress-intensity conditions and this parameter is used in the present study. It should be noted that the increasing K test is not intended to simulate the stresses seen by a welded structure, as a function of time during post-weld-heat treatment, but rather to provide a consistent and carefully controlled method of examining microstructural effects on crack growth resistance. The tests were designed to address the problem of crack growth rather than crack initiation ahead of a notch. In all cases fatigue pre-cracks were grown to a distance of 0.3 mm ahead of the notch, under similar (low mean stress) conditions prior to static loading to facilitate crack

initiation. All static tests were completed in approximately six hours.

Tensile properties were measured for the extremes of heat treated conditions at room temperature and at 500°C, using standard Hounsfield number 11 testpieces. Tests performed at 500°C were completed within a total time of 20 minutes (including the heating-up period). A nominal crosshead displacement rate of 1mm per minute was used. The effects of tempering at 500°C on matrix strength during the actual test period (of up to six hours) were evaluated from room temperature Vickers hardness, V_H , measurements for the extremes of heat treated conditions.

2.3 Metallography

Thin foils were prepared directly from discs machined from the centre of testpiece blanks subjected to the extremes of heat-treatments shown in fig 2 (ie foils were viewed in the as-quenched conditions only). Foil preparation used a jet polisher with an electrolyte of 25% glycerol, 5% perchloric acid, and 70% ethanol at room temperature. Observations were made using a Philips EM300 microscope operating at 100kV.

Prior austenite grain sizes and packet sizes were measured from polished and etched (in 2% Nital) metallographic sections. Sections were viewed optically.

2.4 Fractography

After testing at 500°C, notched-bend testpieces were broken open at low temperatures (typically -196°C) to expose the high-temperature crack surfaces for fractographic analysis. Samples of each heat-treated condition were examined in a CamScan S4 scanning electron microscope (SEM). A high resolution SEM study was also performed on fracture surfaces representing the range of heat-treated conditions in an Hitachi S-570 SEM. Fractographic features were compared at equivalent values of the stress intensity, K , and at equivalent values of the crack growth rate, da/dt .

The size distributions of various fractographic features such as particles and voids, were assessed either manually (graticular

measurements on SEM micrographs) or automatically using an IBAS image analyser. Particles larger than a few hundred nanometres could be identified by energy dispersive X-ray spectroscopy (EDS) in the SEM. Smaller particles were first extracted from fracture surfaces using two-stage replication (acetate and carbon films), and then analysed using EDS in a Philips 400 ST transmission electron microscope.

For two additional testpieces, from the 1300 WQ and 1300-1000 WQ conditions, static crack growth tests were interrupted at a stress-intensity of $52 \text{ MPa}\sqrt{\text{m}}$ by unloading and cooling rapidly to room temperature. Note that the rate of crack growth was carefully controlled for both testpieces, to ensure that the tests were interrupted after an equivalent time (5 hours). Specimens suitable for Auger electron spectroscopy could then be machined from each testpiece to include the high-temperature crack-tip. When broken open in the fracture stage of a Vacuum Generators ESCALAB II Auger system, the crack-tip surface chemistry and the interfacial chemistry of the embrittled grain boundaries immediately in front of the crack-tip, could be analysed and compared with those embrittled boundaries observed to be remote from the crack-tip region. Further details of this procedure are given elsewhere (1, 14).

All Auger electron spectra were obtained in the direct pulse-counting mode ($N(E)$ versus E) using a beam current of 20nA at an accelerating voltage of 10kV. These spectra were then differentiated numerically to provide the more familiar double peaks ($dN(E)/d(E)$ versus E) which were used to quantify the relative concentrations of elements detected.

3. Results

3.1 Crack growth under monotonic loading

The dependence of crack growth rate, da/dt , on the stress intensity K , is shown in figs 3 and 4 for the full range of quenched conditions. In fig 3 a linear relationship between the stress intensity, K and the logarithm of the crack growth rate, $\log (da/dt)$ is observed. A functional relationship of the form:

$$da/dt = Ae^{K^2} \dots \dots \dots (1)$$

where A is a numerical constant, can therefore be suggested. Note, however, that for values of K greater than $\sim 50 \text{ MPam}^{1/2}$, there is some indication of a steeper dependence of crack growth rate on stress intensity - see fig 3. This is more clearly observed if the logarithm of the stress intensity, $\log K$, is plotted versus the logarithm of the crack growth rate, $\log (da/dt)$, see fig 4. The dependence of da/dt on K can be approximated by two straight lines of differing slopes. A functional relationship of the form:

$$da/dt = BK^m \dots \dots \quad (2)$$

can therefore be suggested, where B is a numerical constant and m is the slope of the line. The change in slope is observed for the range of quenched conditions at values of K between 48 and $55 \text{ MPam}^{1/2}$.

Most importantly from figs 3 and 4, it can be seen that, as the final austenitising temperature prior to quenching decreases, the crack growth resistance increases. It is also clear from these figures that the linear elastic stress intensity, K, can be used to characterise crack growth. For the high strength martensitic conditions ($\sigma_0 \sim 540 \text{ MPa}$ at 500°C), it should be noted from Table 2 that the calculated maximum extent of the plastic zone at 500°C is less than 1.5 mm even for an applied stress intensity of $80 \text{ MPam}^{1/2}$. In addition, specimen size requirements for the measurement of fracture toughness, according to BS5447:1977 (16), are met for applied stress intensities approaching $50 \text{ MPam}^{1/2}$, Table 2.

For the two extremes of quenched condition, tensile properties and room temperature hardness values are given in Tables 3 and 4 respectively. Closely similar 0.2% proof stresses and tensile strengths were obtained at both 20 and 500°C . A substantial loss in percentage reduction of area at failure was measured for the 1300 WQ condition alone when tested at 500°C . No such reduction was found for the 1300-90Q WQ condition. Therefore, a decreased resistance to crack growth at 500°C occurred for the 1300 WQ condition in both sharp-crack testpieces and plain tensile testpieces.

The effect of tempering time at 500°C on the room temperature hardness values is shown in Table 4. After 12 h at 500°C, the room temperature hardness fell to 90% of its value prior to tempering in both extremes of quenched condition. Closely similar hardness values were measured for both quenched conditions.

3.2 Metallography

Careful metallographic observations were made for the 1300 WQ and 1300-900 WQ conditions. No significant differences in lath packet sizes or prior austenite grain sizes were detected using optical microscopy. The mean prior austenite grain size was measured as approximately 250 μm for both conditions. Packet sizes were observed to be typically of the order of 100 μm .

Thin-foil transmission electron microscopy confirmed that the microstructure was martensitic in both the 1300 WQ and 1300-900 WQ conditions. A low magnification micrograph of the 1300-900 WQ condition is shown in fig 5. Detailed measurements of lath widths were made directly from such micrographs as shown in fig 6. The measured size distributions of lath widths are shown in fig 7. (The conventions used to determine these widths are noted elsewhere (15)). The mean lath widths are closely similar for the 1300 WQ and 1300-900 WQ conditions, being 89 and 81 nm respectively. This difference in mean lath width is not statistically significant at the 90% confidence level (if a normal distribution is assumed).

Very fine autotempered carbides in the size range 9 to 17 nm were measured for both conditions. Traces of retained austenite could be observed in dark field images from each condition, but these volume fractions were far too small (certainly less than 5%) to allow any quantitative comparison. In summary, the metallographic investigation indicates that the extremes of heat-treatment schedules employed, fig 2, produced similar, uniform, martensitic microstructures

3.3 Fractography

A general SEM examination of the fracture surfaces produced in notched-bend testpieces indicated that the fracture mechanism was 100% intergranular for all quenched conditions. From figs 3 and 4 it is

clear that fracture morphologies can be compared for different quenched conditions at equivalent values of stress intensity, K , and crack growth rate, da/dt .

Consider first the condition directly quenched from 1300°C (1300 WQ). The intergranular facets were smooth over a wide range of stress intensity, $K = 20-50 \text{ MPa}\sqrt{\text{m}}$ and growth rate, $da/dt = 10^{-4} - 5 \cdot 10^{-2} \text{ mm s}^{-1}$.

A typical fractograph is shown in fig 8(a). A closer inspection of such facets reveals "striations" normal to the direction of crack growth as shown in fig 8(b). These striations are spaced approximately 2-9 μm apart. A striation is shown in detail in fig 8(c). Large inclusions ($> 1 \mu\text{m}$ in diameter), were also occasionally observed on these smooth facets, together with numerous fine precipitates (approximately 100 nm in diameter). The large inclusions were identified as manganese sulphides by EDS analysis. Some of the fine precipitates were extracted by two stage acetate/carbon replication and examined using EDS in the TEM. This process involved no acid etching and did not therefore dissolve any of the grain-boundary particles. More than 95% of the particles analysed gave similar X-ray spectra, characteristic of M_3C carbides in 2% Cr-1Mo steel. The average metalloid content was 97.6 wt % Fe, 2.2 wt % Cr and 0.2 wt % Mo.

At the higher stress intensity of 60 MPa $\sqrt{\text{m}}$ and a growth rate of $10^{-1} \text{ mm s}^{-1}$ a clear change in fracture mechanism was observed. The intergranular facets were no longer essentially smooth with striations, but were instead covered with microvoids of two distinct size scales, see fig 9(a). The fine cavities were centred on fine precipitates fig 9(b), identified as M_3C carbides, and the coarser cavities were centred on large particles (200-300 nm in diameter), fig 9(c), identified as manganese sulphides, fig 10. (Note that in order to identify these 200-300 nm particles it was necessary to strip away numerically the matrix contribution to the combined X-ray signal from both matrix and particle).

The 1300-1100 WQ condition exhibited similar fractographic features to those observed above for the 1300 WQ condition. A change in fracture mode was again observed from smooth intergranular (at low stress intensities) to intergranular microvoid coalescence (at higher stress

intensities). For this condition, fine cavitation (around carbides) occurred at lower stress intensities and crack growth rates than coarse cavitation (around inclusions). Fine cavitation (around carbides) occurred at all stress intensities greater than $K = 40 \text{ MPam}^{1/2}$, and crack growth rates greater than $da/dt = 3.10^{-4} \text{ mms}^{-1}$, whereas coarse cavitation around small inclusions occurred only at stress intensities greater than $K = 55 \text{ MPam}^{1/2}$, and crack growth rates greater than $da/dt = 1.10^{-3} \text{ mms}^{-1}$.

For the 1300-900 WQ condition, fine cavitation was observed for stress intensities between $K = 42-55 \text{ MPam}^{1/2}$ and crack growth rates between $da/dt = 5.10^{-5} - 1.10^{-4} \text{ mms}^{-1}$. At stress intensities greater than $K = 55 \text{ MPam}^{1/2}$ coarse-cavitation alone was observed.

For the two extremes of the above conditions, compared at an equivalent crack growth rate of $3.10^{-4} \text{ mms}^{-1}$, increased microductility was associated with the intergranular fracture as the final austenitising temperature decreased, see fig 11.

A change in fracture mode from essentially smooth intergranular facets to intergranular facets exhibiting microductility was observed for all quenched conditions as the stress intensity increased. It is of interest to note that this transition, associated with the onset of coarse cavitation around sulphides, appears to occur at a similar stress intensity of $48-53 \text{ MPam}^{1/2}$ for the range of quenched conditions see, fig 12. In addition, from fig 4, it can be seen that there is a greater dependence (higher value of 'm' - equation 2) of crack growth rate on stress intensity for values of stress intensity greater than $48-55 \text{ MPam}^{1/2}$. From these observations it may be deduced that the onset of IGMVC is responsible for the increased dependence of crack growth rate on stress intensity.

Variations in the size distribution of major fractographic features such as striation spacing, large sulphide diameter and area density, small sulphide diameter, carbide diameter, coarse cavity diameter (around inclusions) and fine cavity diameter (around carbides), were measured as a function of quench condition. The results are given in

Table 5. All particles and voids were assumed to be spherical, and average diameters were calculated from a sample of 50-200 features. Striation spacings were more difficult to quantify and are therefore given as an observed range.

The fractography of tensile specimens tested at 500°C indicated that HTBIGF can also be an important failure mechanism for this testpiece geometry. The 1300-900 WQ condition exhibited occasional partial intergranular facets, whilst for the 1300 WQ condition, HTBIGF covered some 30% of the fracture surface. These observations are consistent with the values of reduction in area given in Table 3.

3.4 Auger electron spectroscopy

Examples of the Auger spectra obtained from testpieces interrupted during high temperature cracking (of the 1300 WQ and 1300-1000 WQ conditions) are shown in fig 13(a) and (b). The interfacial boundaries remote from the highly stressed crack-tip region in both the 1300 WQ and the 1300-1000 WQ conditions comprised iron, oxygen, carbon and segregated phosphorus. An example of a typical spectrum is shown in fig 13(a). Note that these measurements are made on intergranular facets which open up as a consequence of the brittle impact failure within the Auger system, at low temperature (typically - 196°C). These facets are featureless and are therefore clearly different to those produced during brittle high-temperature crack growth, compare fig 14(a) and (b). The average concentration of phosphorus measured on such grain boundaries was 9.0% (peak height ratio to Fe_{703} -phr) with a standard deviation of 1.0% phr for the 1300 WQ condition and 10.5% phr with a standard deviation of 0.8% phr for the 1300-1000 WQ condition. The high-temperature crack surfaces were contaminated with carbon and oxygen and these elements were used to locate those boundaries close to crack-tips. Only those boundaries displaying HTBIGF were examined. In both quenched conditions, significant increases in sulphur concentrations were measured in the crack-tip regions. fig 13(b). Intriguingly, the average surface concentration of sulphur was similar in both quenched conditions at approximately 3.5 atomic % (as calculated using a S:Fe sensitivity ratio of 4.6). In addition to sulphur and phosphorus, nitrogen was also detected at some crack-tip locations in the 1300 WQ condition.

4. Discussion

From figs 3 and 4, it is apparent that the crack growth resistance curves are strongly dependent on the final austenitising temperature prior to quenching. Crack growth resistance increases as the final austenitising temperature decreases. If the 1300 WQ and 1300-900 WQ conditions are compared at equivalent stress intensities, the crack growth rates, da/dt , are at least two orders of magnitude lower for the 1300-900 WQ condition. Note that the matrix strength (Table 3), lath width (fig 7), packet size and prior austenite grain size are closely similar for these two quenched conditions. To explain the observed changes in growth rate with final austenitising temperature prior to quenching, it is therefore necessary to investigate the effect of these heat treatments on the behaviour of trace impurity elements such as sulphur and phosphorus. Both these elements have previously been known to cause embrittlement of grain-boundaries in iron at low temperatures, (17,18,19) and both were observed at embrittled boundaries in the present study, fig 13. Additionally, fine manganese sulphides formed after overheating are known to reduce toughness by embrittling prior austenite grain boundaries on reprecipitation from solution (20).

SAM studies indicate that the concentration of phosphorus at prior austenite grain boundaries was marginally increased for the 1300-900 WQ condition from 9.0% phr to 10.5% phr (see also reference 21). Since increased amounts of phosphorus at grain boundaries have been shown to reduce toughness (18-20), it follows in the present study that phosphorus is not the embrittling species primarily responsible for the high temperature form of intergranular cracking. Attention is now given to the role of sulphur, and it is necessary to address the two forms of cracking observed, namely HTBIGF (at stress intensities less than $\sim 55 \text{ MPam}^{1/2}$) and IGMVC (at stress intensities greater than $\sim 55 \text{ MPam}^{1/2}$).

4.1 High Temperature Brittle Intergranular Fracture (HTBIGF)

Direct evidence of sulphur segregation at crack-tips has been obtained by SAM studies, see fig 13. A more detailed characterisation of such segregation may be found in reference 14. The dynamic nature of the segregation of sulphur to the crack tip under stress may be deduced from the absence of sulphur observed on intergranular facets remote from the crack-tip produced by low temperature impact fracture (within the scanning Auger microprobe). The embrittlement of these boundaries found

in the bulk (ie remote from the crack-tip) of the testpiece is attributed to the segregation of phosphorus alone. It is important to note that these different types of intergranular fracture can be distinguished fractographically - compare figs 14(a) and 14(b). The facets observed in the low temperature (phosphorus assisted) fracture are microscopically smooth, fig 14(b), while those observed in the high temperature (phosphorus and sulphur assisted) fracture exhibit additional striations perpendicular to the direction of crack growth, fig 14(a).

It may be suggested from the striations observed during high-temperature crack growth that a stepwise-growth mechanism is appropriate. This provides positive support for a recent theoretical model for the stress driven diffusion of sulphur to crack-tips (1). For the application of this model it is also of interest to observe from Table 5, that the striation distance is in the range 2-9 μm for all of the heat-treated conditions, stress-intensities and growth rates, and may therefore be taken as approximately constant. These striation spacings do not correspond to the scale of any microstructural features: the lath width was measured as approximately 0.08 μm ; the packet size was measured as 100 μm and the prior austenite grain size as 250 μm . They are, however, broadly consistent with the distances over which sulphur segregation might be influenced by high tensile stresses. Peak tensile stresses will be achieved at a distance of 1.9δ (where δ is the crack-opening displacement) within the plastic zone ahead of the crack tip (22). This distance may be deduced (14) to be an upper limit to the range of the stress assisted segregation of sulphur and is seen from Table 6 to exceed the size of the maximum observed striation spacing.

From the experimental observations it seems probable that sulphur plays a controlling role in the mechanism of HTBIGF at high temperature. It has been shown that the average coverage of sulphur ahead of a crack-tip is closely similar at the same stress intensification level of 52 $\text{MPa}\sqrt{\text{m}}$ for both the 1300 WQ and 1300-1000 WQ conditions. The precise interpretation of such coverage values is considered in detail elsewhere (14), but here it is suggested that there may be a critical coverage of sulphur which is required to promote a step-wise crack advance at a given level of stress intensification.

The source of the sulphur that is observed to concentrate at grain boundaries under stress is not completely resolved and is also considered further in reference (14). It is nevertheless generally accepted that the required rates of sulphur migration can only be achieved by atomistic diffusion. Two possible sources of atomistic sulphur have been postulated:

- (i) that retained in solid solution from the austenitising treatment(1);
- (ii) that produced by the surface dissolution of fine sulphides in vacuo at the test temperature (2, 23). The former hypothesis is based on the results of Turkdogan et al (24), who studied the equilibrium solubility limits of sulphur in iron. The solubility limits are critically dependent on the amount of manganese present. For iron containing 0.53 wt % manganese these equilibrium levels at the austenitising temperatures of interest are given in Table 7, and provide an estimate of the amount of sulphur in solid solution prior to quenching.

In order to comment further it is necessary to consider the possible effect of the quench on the sulphur present in solid solution. For the 1300 WQ condition, the initial level of sulphur in solid solution is 31 ppm, and the rate of quenching will be the most severe. On quenching, some sulphur will reprecipitate from solution onto existing sulphides and/or to form new sulphides. The large degree of undercooling in the severe quench will favour fresh precipitation (large driving force) and the amount left in solid solution will be high (limited diffusion time). For the 1300-900 WQ condition, the initial level of sulphur in solid solution prior to quenching is only 0.4 ppm, and therefore 98.7% of that amount of sulphur in solid solution at 1300°C will have reprecipitated during the slow furnace cool from 1300 to 900°C, fig 2. During the cooling sequence, more reprecipitation onto existing sulphides would be expected because the driving force is reduced and the time for diffusion is greater compared with the quench from 1300°C. For the 1300-1100 WQ condition the distributions of sulphur and sulphides would be predicted to be intermediate between those observed for the 1300 WQ and 1300-900 WQ conditions.

This interpretation is consistent with the quantitative particle analyses given in Table 5. As the severity of quench increases in the

order 1300-900 WQ, 1300-1100 WQ and 1300 WQ: (i) the number density of large sulphides remains approximately constant but their average diameter decreases. This observation is attributed to a decreased amount of precipitation onto existing sulphides during the quench; (ii) the average diameter of small sulphides remains approximately constant, but their number density increases (this assumes that the number density of sulphides is inversely proportional to the coarse-void diameter and is valid provided that there is a direct one-to-one correlation between number of coarse-voids and number of sulphide inclusions). This observation is attributed to the promotion of fresh precipitation as the severity of the quench is increased.

The quantitative measurements given in Table 5, would predict increased crack growth rates for the 1300 WQ condition either (a) because of the increased amount of sulphur present in solid solution (1), or (b) because of the increased density of fine sulphides (2, 23) and it is not possible therefore to establish the primary source of atomistic sulphur from these observations alone. Some recent results (14) do, however, firmly indicate the importance of the amount of sulphur present in solid solution.

4.2 Intergranular Microvoid Coalescence (IGMVC)

This mechanism of crack growth proceeds by the nucleation, growth and coalescence of voids centred largely on small manganese sulphides which are associated with grain boundaries. The transition from HTBIGF to IGMVC appears to occur at a closely similar stress intensification of $48-55 \text{ MPam}^{1/2}$ for the range of heat-treatments considered. The mechanism of IGMVC will be critically dependent on the size and spatial distribution of sulphides, and the growth rates at this transition correlate with the distribution of sulphides observed in Table 5. As the severity of quench increases in the order 1300-900 WQ, 1300-1100 WQ and 1300 WQ, the growth rate at the transition point also increases. This is consistent with the observed increase in density of small sulphides, which is proportional to the reciprocal of the void diameter, see Table 5. The mechanism of IGMVC exhibits a steeper dependence of crack growth rate on stress intensity (see fig 4) for $K \leq 48-55 \text{ MPam}^{1/2}$, than that observed for HTBIGF.

4.3 The Transition from HTBIGF to IGMVC

The above discussion has suggested that the mechanism of HTBIGF is primarily controlled by the diffusion of sulphur to crack-tips, whereas the mechanism of IGMVC is largely controlled by the size and spatial distribution of sulphides. Fig 15 gives a schematic representation of these mechanisms. For simplicity the role of carbides is not represented in fig 15, although voids have been observed around them, fig 9(b). Small sulphides, reprecipitated from solid solution, are considered to lie a short distance away from the grain boundary, consistent with previous transmission electron microscope observations (25), and do not appear in HTBIGF. Large sulphides do intersect the grain boundary and are therefore observed in HTBIGF, as shown in figs 8(b) and 14(a).

The transition from HTBIGF to IGMVC is observed to occur at stress intensities in the range 48-55 MPam^{1/2}, figs 4 and 12. From Table 2, it can be seen that the specimen size requirements for the measurement of a valid fracture toughness value are just met at such stress intensities. Therefore, excessive plasticity or loss of constraint is not thought to be responsible for the transition from HTBIGF to IGMVC, but there remains the possibility that this transition could be specimen size dependent. It is suggested that as the applied stress intensity rises to a level 48-55 MPam^{1/2}, voids nucleated on the small sulphides adjacent to grain-boundaries grow sufficiently fast to intersect the grain-boundaries in the intervening time between 'jumps' in the stepwise HTBIGF process, see fig 15. This is consistent with a higher growth rate exponent 'm' (equation 2) associated with the IGMVC process. The result is an effective blunting of the sharp HTBIGF crack tip, leading to a transition to the microvoid based mode of intergranular fracture, IGMVC.

It is not possible to comment further on the level of stress-intensity at which the transition occurs without a more detailed understanding of the location of small grain-boundary sulphides (14).

4.4 Theoretical Model for HIBIGF

A recent study by Hippley, Rauh and Bullough (1) has suggested that the average coverage of solute atoms per unit area of crack-surfaces, P , is given by:

$$P = N(\Delta t)/2 v \Delta t \dots\dots (3)$$

where $N(\Delta t)$ is the number of solute atoms that have reached the crack surface in time Δt and v is the crack growth rate. Moreover, $N(\Delta t)$ is proportional to:

$$N(\Delta t) \propto C_0 (KD \Delta t/k_p T)^{4/5} \dots\dots (4)$$

where C_0 is the bulk concentration of solute, K is the stress intensity, k_p is Boltzmann's constant, T is the temperature, and D is the diffusion coefficient.

The observations have suggested that the jump-distance Δa , is approximately constant for all heat-treatments considered. Since

$$v = \Delta a/\Delta t \dots\dots (5)$$

and $T, D, \Delta a$ are constant at each test temperature, it then follows by rearranging equations 3, 4 and 5, that the average coverage is given by:

$$P \propto C_0 (K/v)^{4/5} \dots\dots (6)$$

If an estimate of C_0 for the heat-treatment considered can be made from Turkdogan (24), see Table 7, it is possible to estimate the variation of coverage P , for any given combination of stress intensity, K , and crack growth rate, v . The parameter $F = C_0 (K/v)^{4/5}$ where $F \propto P$, is plotted versus stress intensity, K , in fig 16. From this figure it may be deduced that there is a critical coverage which is required to promote step-wise crack growth for a given level of stress intensification. This is consistent with the average concentration of 3.5 atomic % sulphur observed for both 1300 WQ and 1300-1000 WQ

conditions which were loaded under similar stress intensities. Using this measured value of sulphur concentration and assuming a linear dependence on P , it is possible to replot fig 16 in terms of mean sulphur concentration against stress intensity as shown in fig 17. The broken line in fig 17 indicates that the mechanism of IGMVC dominates over this range of stress intensity and the predicted sulphur concentration would therefore be an underestimate. The form of this curve is similar to that obtained in studies of classical temper embrittlement (18, 19).

The results obtained in the present study appear to support the basic concept of the model for solute segregation to crack tips, and to suggest that a critical concentration of sulphur is required to promote stepwise crack advance in HTBIGF.

Conclusions

1. Coarse-grained martensitic microstructures are susceptible to high-temperature intergranular crack growth, in vacuum at 500°C under static loading. Carefully controlled heat-treatment schedules have been used to show that as the final austenitising temperature prior to quenching decreases, crack growth resistance increases for martensitic microstructures of closely similar strength, prior austenite grain size, packet size and lath width.
2. At low stress intensities, up to approximately $48-55 \text{ MPam}^{1/2}$, the mode of crack growth is a low-ductility type of intergranular fracture (HTBIGF), and is controlled by the dynamic segregation of sulphur to crack-tip regions. Crack advance appears to take place by a series of successive discrete jumps which occur when a critical concentration of sulphur (driven by crack-tip stress) is achieved over the jump distance. The observed jump distance does not correspond to any microstructural feature, such as the lath width or packet size, but is consistent with the scale of influence of high tensile stresses which are produced ahead of the crack-tip.
3. At high stress intensities, greater than approximately $55 \text{ MPam}^{1/2}$, the mechanism of fracture changes to intergranular microvoid coalescence (IGMVC), and is controlled by the distribution of sulphides. Of primary importance are the fine sulphides that reprecipitate from solid solution during the austenitising treatment. The transition from HTBIGF to IGMVC is observed to

occur over a critical range of stress-intensity from 48 to 55 MPa \sqrt{m} , and is accompanied by a steeper dependence of crack growth rate on stress intensity. It is suggested that this transition is controlled by a balance between the rate of HTBIGF crack growth, and hence dynamic crack-tip sulphur segregation, and the rate of sulphide-nucleated microvoid growth in front of the crack tip in the period of time between HTBIGF steps.

Acknowledgments

One of the authors (PB) was supported in the course of this work by a SERC post doctoral award, and by a Goldsmith's Junior Research Fellowship at Churchill College, Cambridge. Further support from the Department of Trade and Industry and the Underlying Research Programme of the UKAEA is also gratefully acknowledged. The authors are indebted to Dr H K D Bhadeshia for assistance with the transmission electron microscopy and to Dr J F Knott for helpful discussions. Thanks are also due to Professor D Hull for the provision of research facilities.

References

1. C A Hipsley, H Rauh and R Bullough. *Acta Metall.*, 32, 1381 (1984).
2. J Shin and C J McMahon, Jr. *Acta Metall.*, 32, 1535 (1984).
3. C A Hipsley. *Mater Sci and Tech.*, 1, 475 (1985).
4. C J McMahon, Jr. "Advances in Fracture Research - ICF6", Valluri et al eds, p 143, Pergamon (1984).
5. P Bowen, C A Hipsley and J F Knott. "Fracture Control of Engineering Structures - ECF6", H C van Elst and A Bakker eds, p 1927 (1986).
6. J C Ritter and R McPherson. *Met Tech.*, 1, 506 (1974).
7. C J McMahon, Jr, R J Dobbs and D H Gentner. *Mater Sci and Eng.*, 37, 179, (1979).
8. J Shin, J Kameda and C J McMahon, Jr. "Micro and Macro Mechanisms of Crack Growth" Sadananda et al eds, p 149, TMS-AIME (1981).
9. C A Hipsley, J F Knott and B C Edwards. *Acta Metall.*, 28, 869 (1980).
10. C A Hipsley, J F Knott and B C Edwards. *Acta Metall.*, 30, 641 (1982).
11. P Veron, C A Hipsley and J F Knott. *Int Journ Press Vess and Piping*, 16, 29 (1984).
12. C A Hipsley. *Met Sci.*, 17, 277 (1983).
13. P Bowen, PhD Thesis, Univ of Cambridge (1984).
14. C A Hipsley, submitted to *Acta Metall.*, October 1986.
15. P Bowen and J F Knott. *Met Sci.*, 18, 225 (1984).
16. "Plane Strain Fracture Toughness Testing of Metallic Materials, BS5447:1977.
17. Pichard, J. Rieu and C Goux: *Mem Scient Revue Metall.*, 70, 13 (1973).
18. M L Jokl, J Kameda, C J McMahon, Jr. and V Vitek. *Met Sci.*, 14, 375 (1980).
19. C J McMahon Jr, et al, "Developments in Fracture Mechanics - 2", ed G G Chell, Applied Science, London (1981).
20. B Cane and C J Middleton. *Met Sci.*, 15, 295, (1981).
21. P Bowen, C A Hipsley and J F Knott. *Acta Metall.*, 32, 637 (1984).
22. J R Rice and M A Johnson: "Inelastic behaviour of solids", ed M Kanninen et al, McGraw-Hill, New York, p 641 (1970).
23. I W Chen: *Acta Metall.*, 34, 1335 (1986).

24. E Turkdogan, S Ignatovic and J Pearson. J Iron Steel Inst,
190, 349 (1955)
25. C A Hipsley: Met Sci, 15, 137 (1981).
26. ASME Code for Chemical Plant and Petroleum Refinery Piping,
ANSI/ASME-B31.3a (1981).

TABLE 1

Composition of 2%Cr-1Mo plate, wt. %

Cr	Mo	Mn	Si	Ni	C	P	S
2.12	0.95	0.53	0.17	0.20	0.13	0.015	0.021

TABLE 2

Calculated size of plastic zone, r , and specimen size restrictions, $2.5 (K/\sigma_0)^2$ as a function of applied stress intensity, K , at 500°C

$K(\text{MPa}\sqrt{\text{m}})$	$r(\text{mm})$	$2.5 (K/\sigma_0)^2(\text{mm})$
20	0.09	1.4
30	0.20	3.2
40	0.36	5.7
50	0.57	8.8
60	0.81	12.8
70	1.11	17.4
80	1.45	22.7

TABLE 3

Tensile properties measured for extremes of quenched conditions

Condition	Test Temperature (°C)	$\sigma_{0.2}$ MPa	σ_{UTS} MPa	Reduction of area (%)
1300 WQ	20	1060	1260	56
1300-900 WQ	20	1060	1250	57
1300 WQ	500	820	960	11
1300-900 WQ	500	870	1010	42

TABLE 4

Room temperature Vicker's hardness, V_H (30 kg), as a function of tempering time at 500°C (standard deviations are in parentheses).

Condition	V_H values measured after tempering at 500°C (hours)					
	0	1	2	4	8	12
1300 WQ	406(7)	373(2)	370(6)	364(4)	366(4)	360(4)
1300-900 WQ	409(7)	375(2)	370(4)	368(4)	368(2)	368(2)

TABLE 5

Quantitative analysis of fractographic features
(standard deviations in parentheses)

Feature		1300 WQ	1300-1100 WQ	1300-900 WQ
Striations	Spacing (μm)	2-5	3-7	3-9
Large sulphides	Area density (per $1000\mu\text{m}^2$ of grain boundary)	2.6(0.3)	2.7(0.3)	2.3(0.3)
Large sulphides	Average diameter (μm)	1.15(0.6)	1.35(0.7)	1.50(0.5)
Small sulphides	Average diameter (nm)	190(60)	165(50)	170(60)
Carbides	Average diameter (nm)	74(30)	70(20)	Not analysed
Coarse voids (around sulphides)	Average diameter (μm)	0.68(0.3)	1.15(0.5)	1.40(0.6)
Fine voids (around carbides)	Average diameter (nm)	220(60)	Observed but not measured	Not observed

TABLE 6

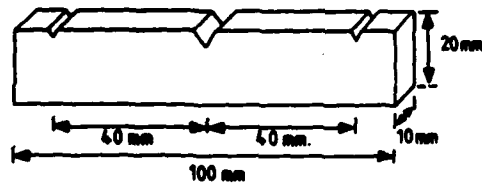
Calculated size of crack opening displacement (δ) at
500°C. using $\delta = K^2(1 - \nu^2)/2\sigma_0 E$, where $\nu = 0.3$,
 $\sigma_0 = 840$ MPa and $E = 169$ GPa (26)

K (MPa \sqrt{m})	δ (μm)	1.95 (μm)
20	1.3	2.5
30	2.9	5.5
40	5.1	9.7
50	8.0	15.2
60	11.5	21.9

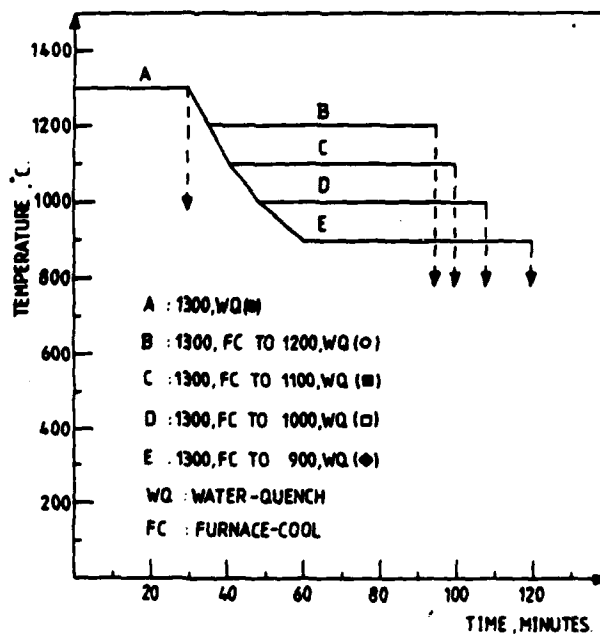
TABLE 7

Equilibrium concentration (C_0) of sulphur in iron
containing 0.53 Mn (wt.%)

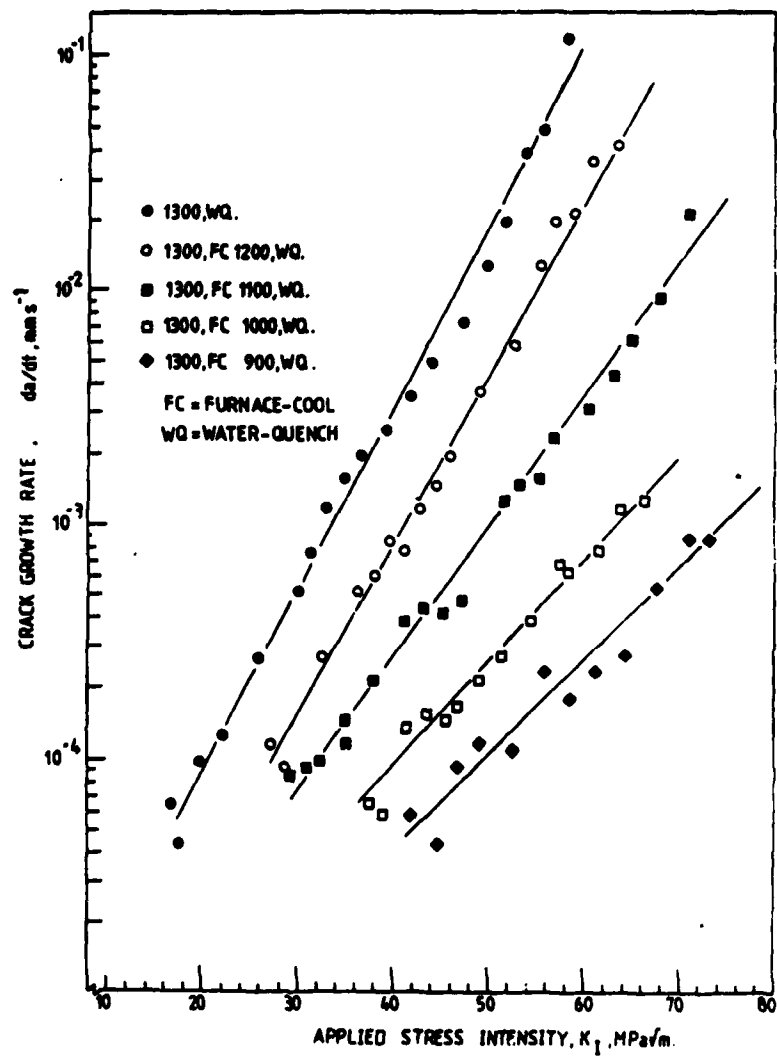
	Temperature (°C)				
	1300	1200	1100	1000	900
C_0 (ppm)	31.0	12.8	4.7	1.4	0.4



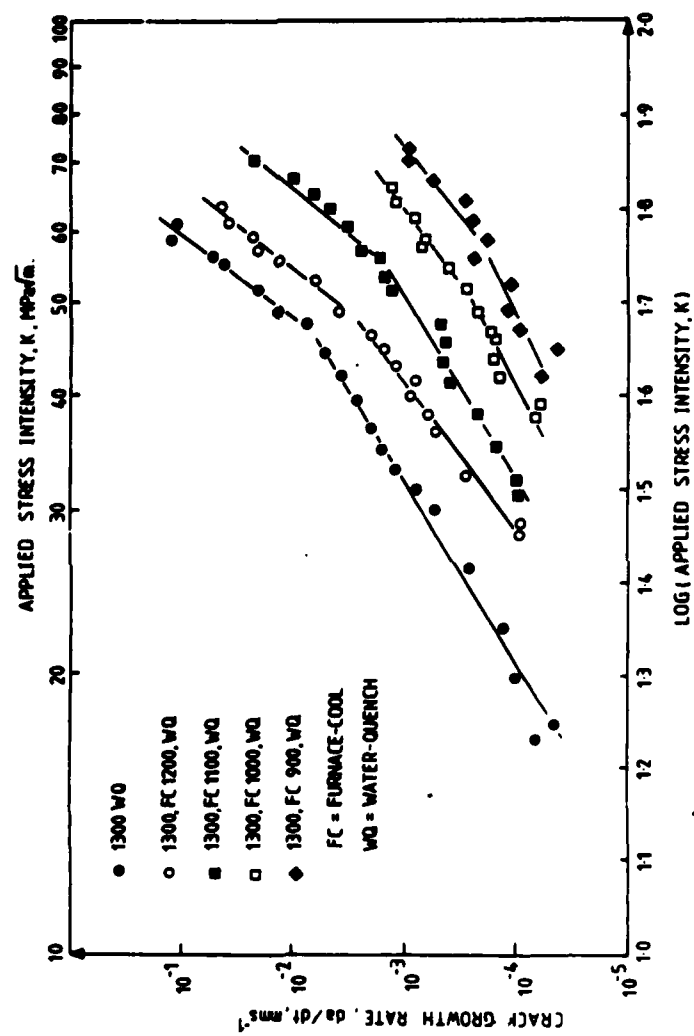
AERE R 12464 Fig. 1
Notched band testpiece



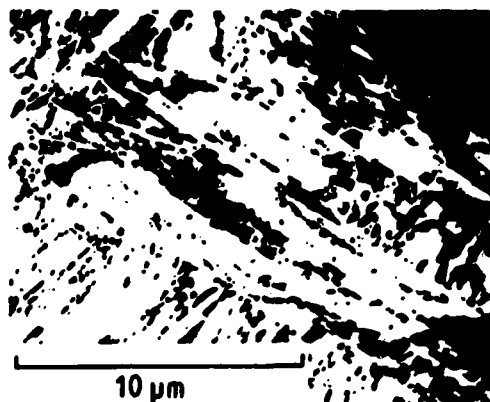
AERE R 12464 Fig. 2
Heat-treatment schedules



AERE R 12464 Fig. 3
 Crack growth resistance curves: stress intensity versus log (crack growth rate)



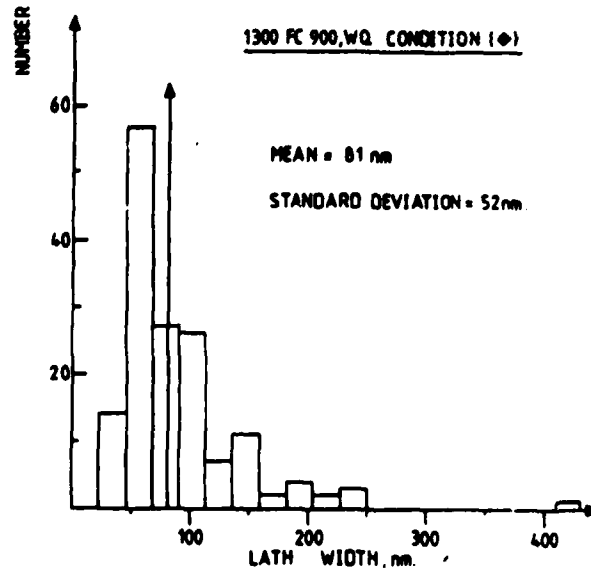
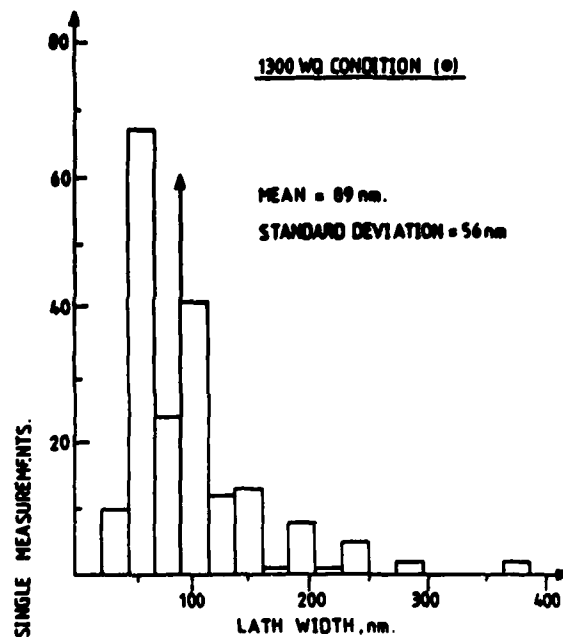
AERE R 12464 Fig. 4
Crack growth resistance curves: log (stress intensity) versus log (crack growth rate)



AERE R 12484 Fig. 5
Low magnification TEM micrograph of 1300-900 WO
condition



AERE R 12484 Fig. 6
High magnification TEM micrograph of 1300 WO
condition



AERE R 12484 Fig. 7
Measured size distribution of lath widths for 1300 WQ and 1300-900 WQ conditions



(a)



(b)



(c)

AERE R 12464 Fig. 8
1300 WQ condition, $K = 40 \text{ MPam}^{1/2}$ (a) general area, (b) striations on individual grain boundary
(direction of crack growth is arrowed) and (c) detail of individual striation arrowed

HARWELL LABORATORY
PHOTOGRAPHIC GROUP

HR 30341

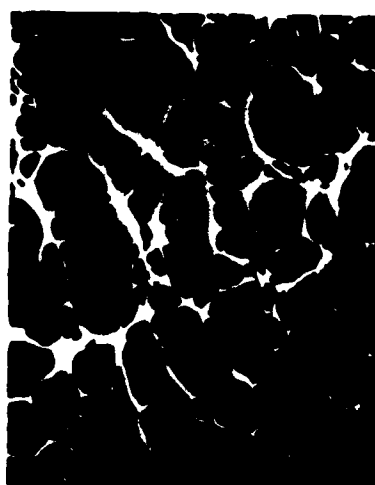




(a)



(b)

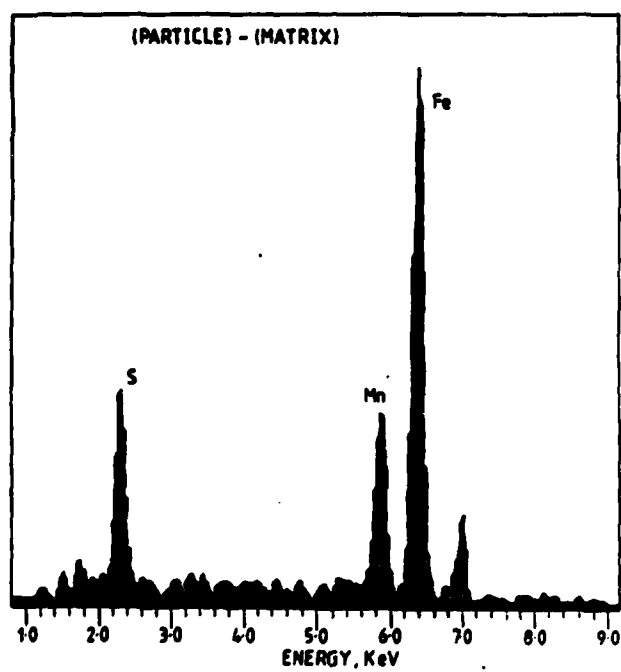


(c)

AERE R 12484 Fig. 9
 1300 WQ condition, $K = 60 \text{ MPam}^{1/2}$ (a) individual grain boundary showing microductility, (b) fine
 cavitation (around carbides, region A) and (c) coarse cavitation (around fine sulphides, region B)

HARWELL LABORATORY
PHOTOGRAPHIC GROUP
HR 30339





AERE R 12464 Fig. 10
EDS spectrum obtained from manganese sulphide inclusion
(= 200 nm)




(a)

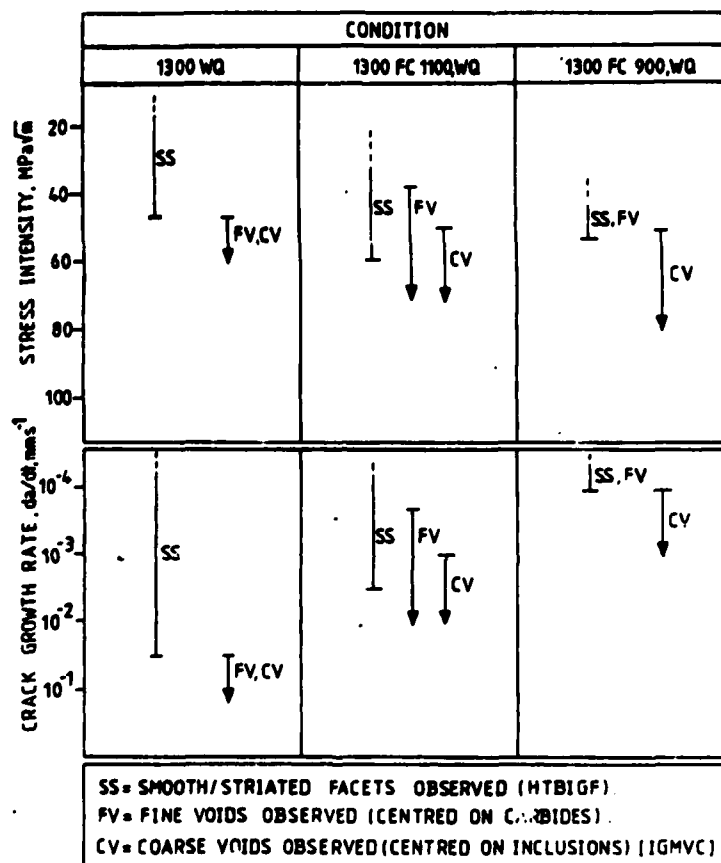


(b)

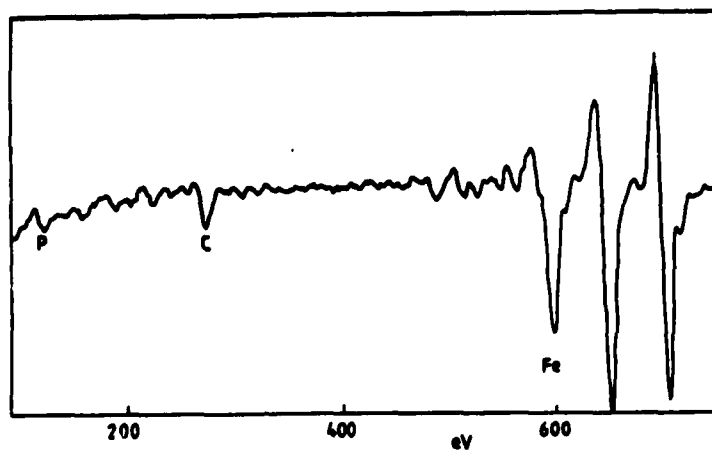
AERE R 12464 Fig. 11
Crack growth rate of 3.10^{-4} mms⁻¹
(a) 1300 WQ condition and
(b) 1300-900 WQ condition

HARWELL LABORATORY
PHOTOGRAPHIC GROUP
HR 30340

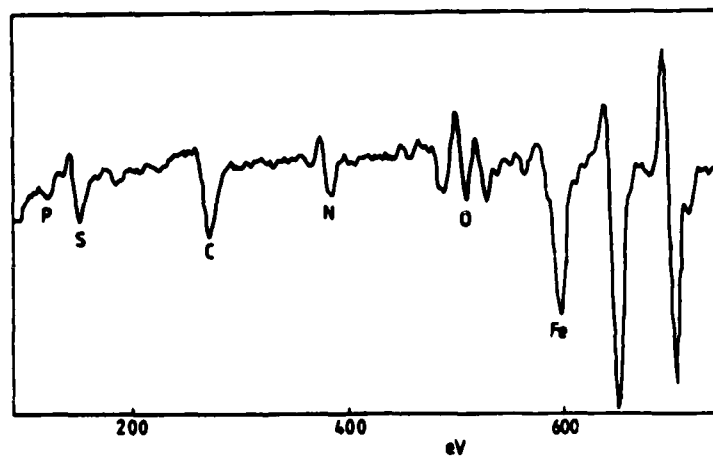




AERE R 12464 Fig. 12
 Summary of observed dependence of fractographic features on (a) stress intensity and (b) crack growth rate



(a) SURFACE CHEMISTRY REMOTE FROM HIGHLY STRESSED CRACK-TIP



(b) SURFACE CHEMISTRY CLOSE TO HIGHLY STRESSED CRACK-TIP

AERE R 12484 Fig. 13

Auger electron spectra [$dN(E)/d(E)$ versus E] obtained from (a) bulk intergranular facet and (b) intergranular facet located at the crack-tip



(a)



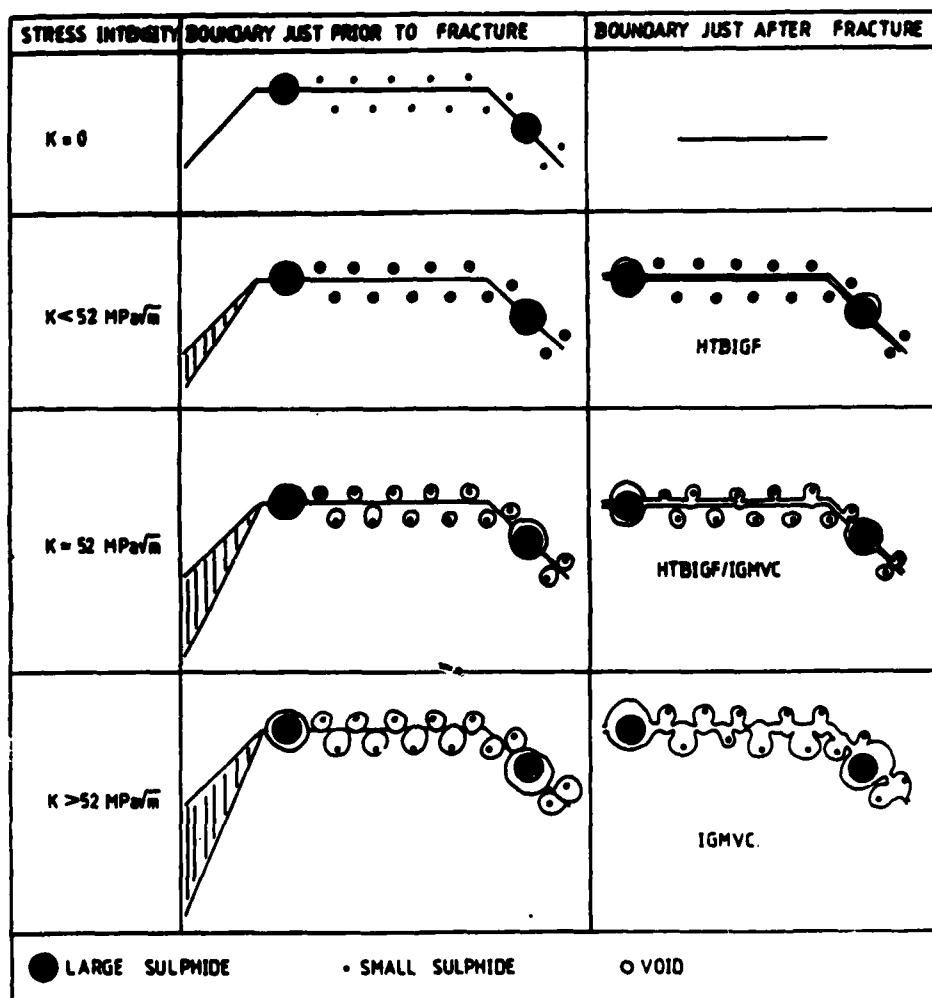
(b)

AERE R 12464 Fig. 14
Comparison of fractographic features
observed on grain boundaries (a) subjected to
HTBIGF at 500°C (direction of crack growth
arrowed) and (b) impact fracture at 196 C

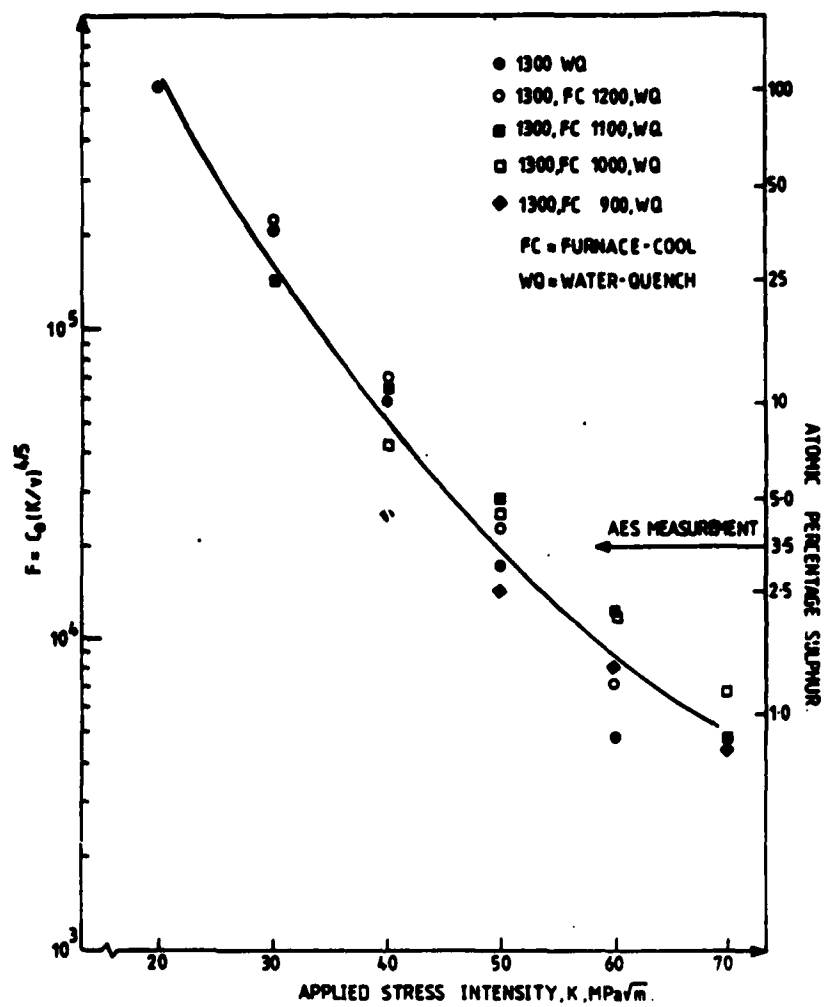
HARWELL LABORATORY
PHOTOGRAPHIC GROUP
HR 30338

[REDACTED]

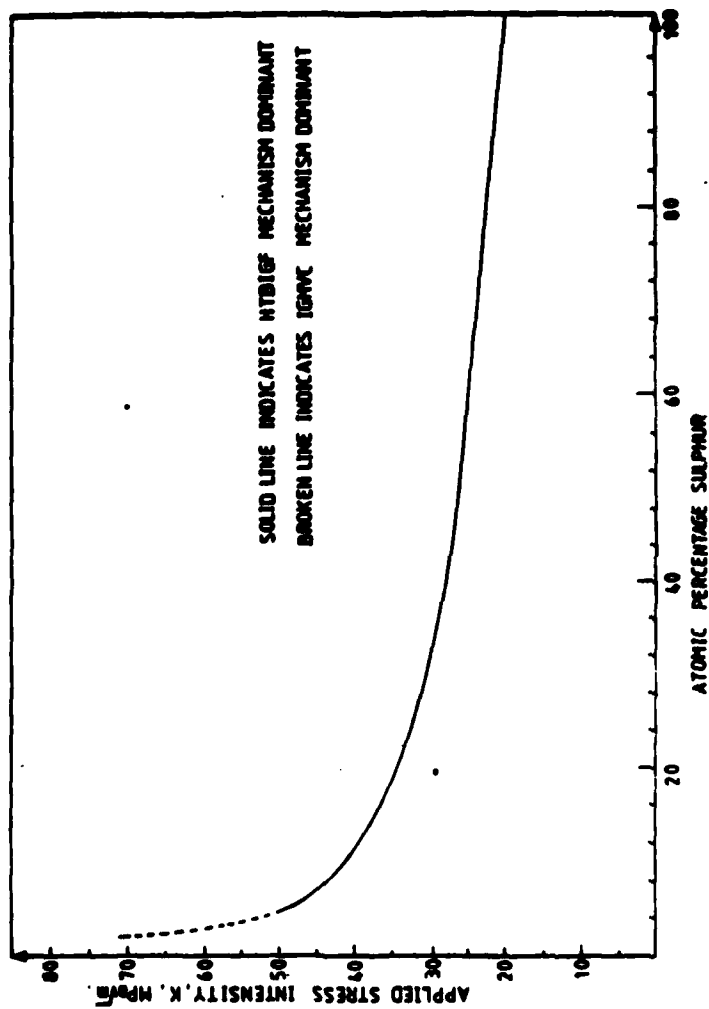
[REDACTED]



AERE R 12464 Fig. 15
Schematic representation of mechanisms of intergranular crack growth



AERE R 12464 Fig. 16
 Calculated coverage (F) versus applied stress intensity (K) for the range of quenched conditions



AERE R 12484 Fig. 17
 Calculated average concentration of sulphur (atomic %) required to promote grain boundary fracture for a range of applied stress intensity

END
FILMED MARCH 1987

END

DATE

~~FILED~~ MED

4 8R